JOURNAL OF NATURAL PRODUCTS

pubs.acs.org/jnp

Article

The Sea Cucumber *Thyonella gemmata* Contains a Low Anticoagulant Sulfated Fucan with High Anti-SARS-CoV-2 Actions against Wild-Type and Delta Variants

Rohini Dwivedi, Marwa Farrag, Poonam Sharma, Deling Shi, Anter A. Shami, Sandeep K. Misra, Priya Ray, Jayanti Shukla, Fuming Zhang, Robert J. Linhardt, Joshua S. Sharp, Ritesh Tandon, and Vitor H. Pomin*

Cite This: *J. Nat. Prod.* 2023, 86, 1463−1475

Read Online

ACCESS | Metrics & More | Article Recommendations | Supporting Information

ABSTRACT: In this work, we isolated two new sulfated glycans from the body wall of the sea cucumber *Thyonella gemmata*: one fucosylated chondroitin sulfate (TgFucCS) (17.5 ± 3.5% kDa) and one sulfated fucan (TgSF) (383.3 ± 2.1% kDa). NMR results showed the TgFucCS backbone composed of [→3)-*β*-*N*-acetylgalactosamine-(1→4)-*β*-glucuronic acid-(1→] with 70% 4-sulfated and 30% 4,6-disulfated GalNAc units and one-third of the GlcA units decorated at the C3 position with branching *α*-fucose (Fuc) units either 4-sulfated (65%) or 2,4-disulfated (35%) and the TgSF structure composed of a tetrasaccharide repeating unit of [→3)-*α*-Fuc2,4S-(1→2)-*α*-Fuc4S-(1→3)-*α*-Fuc2S-(1→3)-*α*-Fuc2S-(1→]$_n$. Inhibitory properties of TgFucCS and TgSF were investigated using SARS-CoV-2 pseudovirus coated with S-proteins of the wild-type (Wuhan-Hu-1) or the delta (B.1.617.2) strains and in four different anticoagulant assays, comparatively with unfractionated heparin. Molecular binding to coagulation (co)-factors and S-proteins was investigated by competitive surface plasmon resonance spectroscopy. Among the two sulfated glycans tested, TgSF showed significant anti-SARS-CoV-2 activity against both strains together with low anticoagulant properties, indicating a good candidate for future studies in drug development.

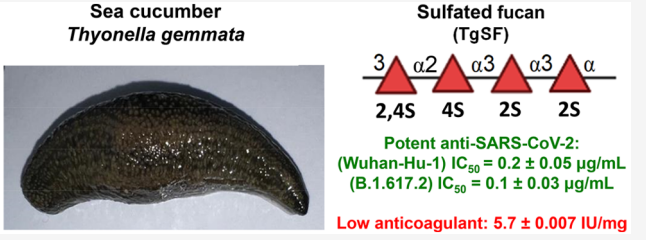

Multiple mutations in the key proteins of severe acute respiratory syndrome coronavirus-2 (SARS-CoV-2) have led to the evolution of numerous variants of concern (VOC).[1] Among all VOCs that have appeared from mutation on the wild type (Wuhan-Hu-1), those containing evolutionary advantages, such as alpha, beta, gamma, delta, and omicron, have shown to cause higher infectivity and mortality rates across the globe.[2] In particular, delta and omicron variants have shown severe pathological consequences to the society.[1] Immune evasion and escape by these continuously emerging VOCs challenge the effectiveness of the available vaccines, requiring timely boosters to increase the antibody protection.[3] The presence of RNA proofreading in the SARS-CoV-2 genome causes low mutation rates compared to other RNA viruses like the human immunodeficiency virus.[4] This leads to the slow but inevitable evolution of SARS-CoV-2 variants, which necessitates development of novel modalities of therapeutic treatment along with vaccine-based immune protection.[5]

SARS-CoV-2 virus functions by attaching to the host-cell surface heparan sulfate proteoglycans (HSPGs) through its spike-protein (S-protein) receptor binding domain (RBD), followed by binding to the human angiotensin converting enzyme 2 (ACE2) receptor, which causes internalization and subsequent infection.[6] This primary interaction is a critical target for therapeutic interventions.[7,8] Other groups and our own have recently shown that competitive disruption of this initial binding complex (S-protein-HSPG) can be achieved by exogenously adding heparin (or mimetics), marine sulfated glycosaminoglycans (GAGs), and synthetic or natural GAG mimetics.[6,9−12] Interestingly, sulfated glycans have been able to inhibit the infectivity of certain VOCs such as delta and omicron,[9,12,13] which is a major advantage in drug discovery.

Nonetheless, potential anticoagulant effects of marine sulfated glycans pose a challenge in the application of these molecules as future antivirals, despite their lower bleeding risks as compared to heparin.[10] Anticoagulant activity of sulfated glycans is an outcome of a combination of specific structural features like sulfation pattern, molecular weight (MW), charge density, glycosidic linkage, and monosaccharide composition. These structural features of sulfated glycans vary in a species-specific manner. This variation, while contributing to the

Received: February 21, 2023
Published: June 12, 2023

https://doi.org/10.1021/acs.jnatprod.3c00151
J. Nat. Prod. 2023, 86, 1463−1475

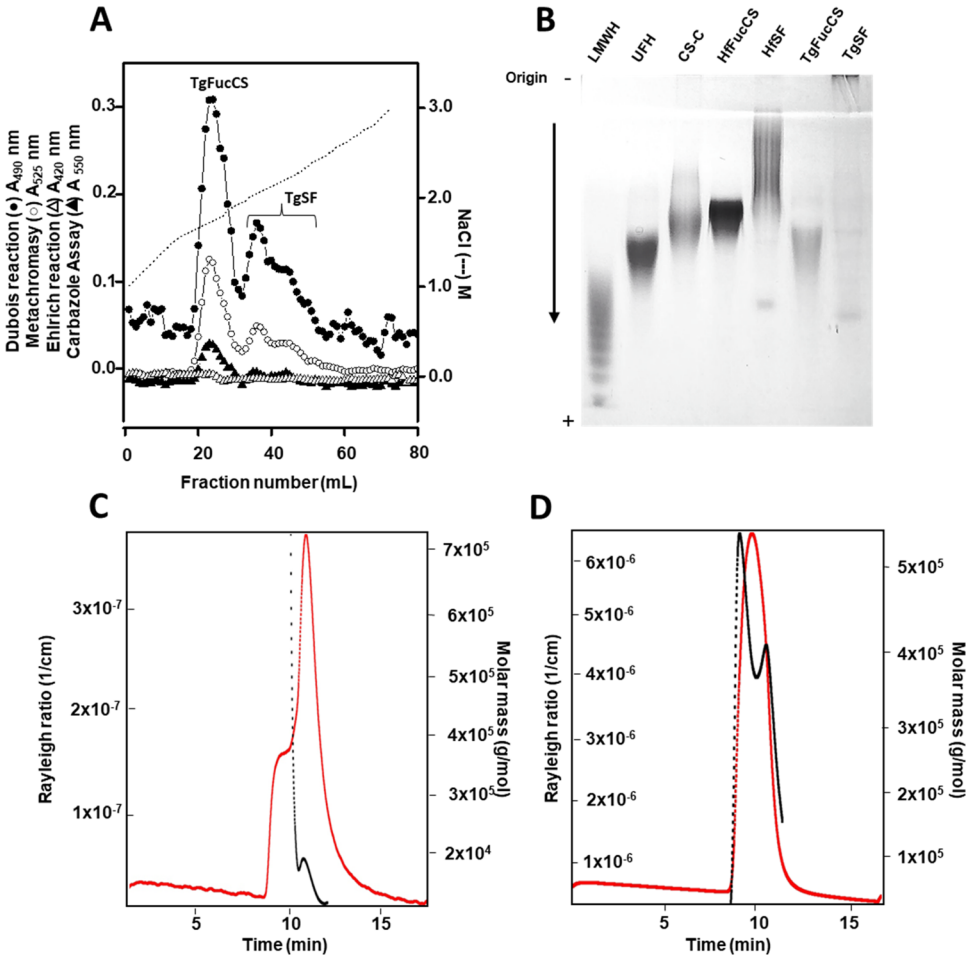

Figure 1. Purification, electrophoretic mobility, and MW estimation of the polyanionic glycosidic fractions obtained from the body wall of the sea cucumber *T. gemmata*. (A) Purification chromatogram indicating two sulfated glycan peaks, labeled as *T. gemmata*-derived fucosylated chondroitin sulfate (TgFucCS) and the *T. gemmata*-derived sulfated fucan (TgSF). (B) Native polyacrylamide gel electrophoresis of TgFucCS and TgSF with standards of known MWs. HPSEC-MALS elution of TgFucCS (C) and TgSF (D) showing MW distribution (black) and Rayleigh ratio (1/cm) (red) versus elution time. UFH, unfractionated heparin; LMWH, low molecular weight heparin; CS-C, chondroitin sulfate C.

structural diversity of these glycans in nature, sometimes also endows these molecules with selective biological functions.[14] Therefore, isolation and exploration of more sulfated glycans with differing structural and functional properties is highly relevant. It increases the prospects of identifying naturally occurring low-anticoagulant molecules endowed with high-antiviral activities like the sulfated fucan from the sea cucumber *Isostichopus badionotus*.[10,15]

Fucosylated chondroitin sulfates and sulfated fucans are examples of unique marine sulfated glycans that are important components of the connective tissue present in the dermis of echinoderms like sea cucumbers. These sulfated glycans play a crucial role in regulating rapid and reversible stiffness changes occurring in the body of these echinoderms.[16] Interestingly, their chemical structures also enable them to exhibit multiple bioactivities such as anticoagulant, antiviral, antitumor, and antimicrobial actions.[17,18] In this work, we isolated and structurally and functionally characterized the two sulfated glycans [one fucosylated chondroitin sulfate (TgFucCS) and one sulfated fucan (TgSF)] from the body wall of the sea cucumber *Thyonella gemmata*. The structural details of both the molecules were investigated by nuclear magnetic resonance (NMR) spectroscopy. Their MWs were assessed by high-performance size exclusion chromatography (HPSEC)-multi-angle light scattering (MALS). The anticoagulant potencies of TgSF and TgFucCS were assessed by both activated partial thromboplastin time (aPTT) and inhibitory assays using purified (co)-factors. The anti-SARS-CoV-2 activities of TgSF and TgFucCS were assessed against the wild-type and delta variants in a pseudovirus-based assay performed in a baculoviral system using GFP-encoding S-protein. Cytotoxic analyses were also conducted. The molecular binding of these holothurian molecules was mechanistically investigated by competitive surface plasmon resonance (SPR) spectroscopy using the purified blood (co)-factors and S-protein RBDs in solution. All experiments were conducted using unfractionated heparin (UFH) as comparative molecule. Among the sulfated glycans examined herein, TgSF showed the best balance of low-anticoagulant side-effects and high-anti-SARS-CoV-2 action against both wild-type and delta strains. This set of results indicates TgSF as a good candidate in future studies regarding novel anti-SARS-CoV-2 sulfated glycans.

RESULTS AND DISCUSSION

Purification, Biochemical and MW Analyses of TgFucCS and TgSF. The dried body wall of the sea cucumber *T. gemmata* was subjected to proteolytic digestion using papain. A 5% (w/w) crude yield of a polysaccharide

https://doi.org/10.1021/acs.jnatprod.3c00151
J. Nat. Prod. 2023, 86, 1463−1475

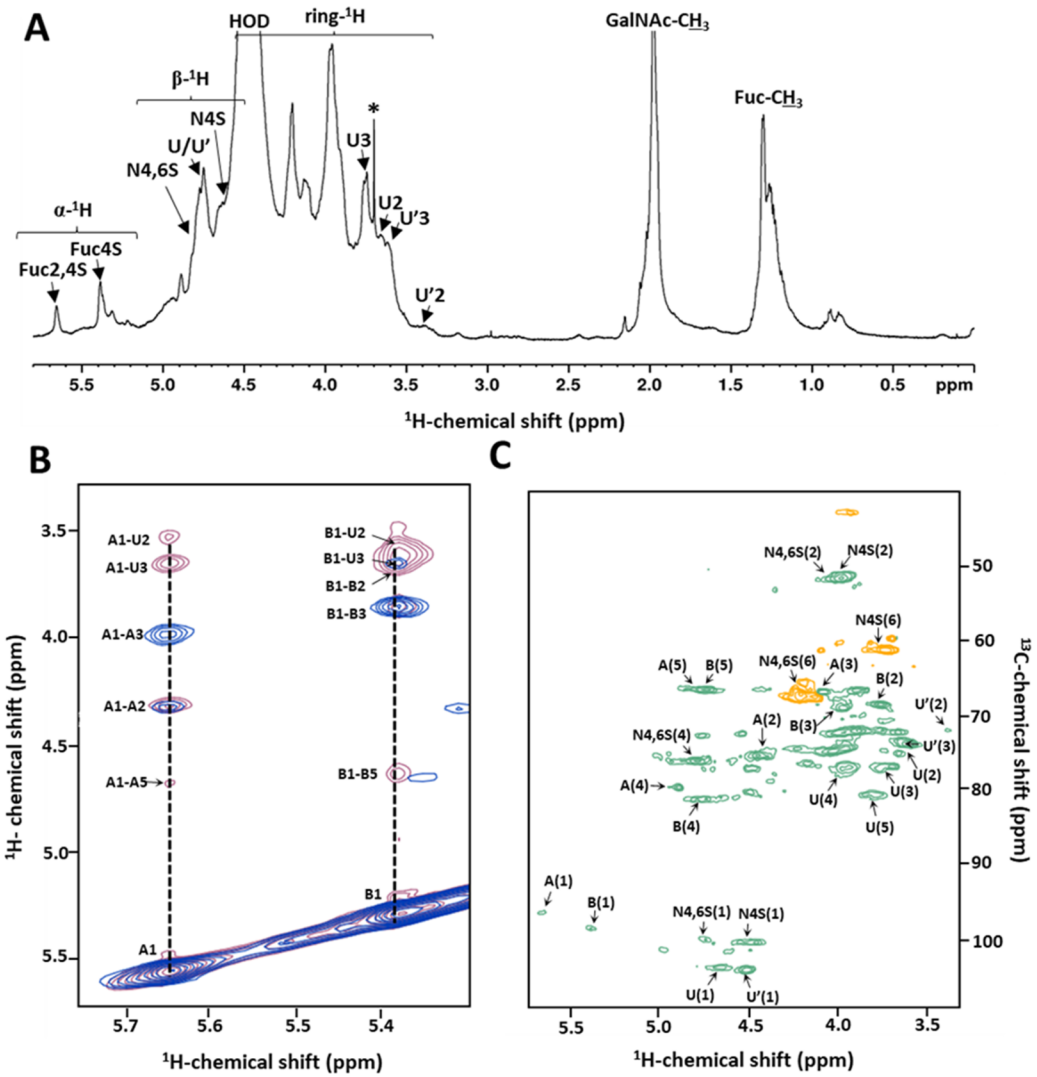

Figure 2. 1D ^{1}H, 2D ^{1}H−^{1}H and ^{1}H−^{13}C NMR spectra of the composing units of TgFucCS. (A) ^{1}H NMR spectrum showing anomeric ^{1}H signals for α-Fuc (labeled as A-Fuc2,4S and B-Fuc4S), β-GlcA (labeled as U-fucosylated GlcA and Ù-nonfucosylated GlcA), and β-GalNAc (labeled as N-GalNAc4,6S and Ǹ-GalNAc4S) as well as GalNAc- and Fuc-methyl protons. (B) The overlaid TOCSY (blue) and NOESY (red) strip showing Fuc spin systems. (C) ^{1}H−^{13}C HSQC spectrum showing the ^{1}H−^{13}C cross-peaks of the composing sugar rings. Numbers in parentheses denote the corresponding proton or carbon atoms. Fuc, GlcA, GalNAc, and S stands for fucose, glucuronic acid, *N*-acetylgalactosamine, and sulfation, respectively.

mixture was obtained. The crude mixture was fractionated by anion-exchange chromatography on a DEAE Sephacel column, using a linear gradient (from 1 to 3 M) of NaCl solution (Figure 1A). Collected fractions were assayed for the presence of hexose (solid circle, Figure 1A), sulfation (open circle, Figure 1A), uronic acid (solid triangle, Figure 1A), and sialic acid (open triangle, Figure 1A). Two populations of polysaccharides, TgFucCS and TgSF, with starting elution around ∼1.6 and ∼2.0 M NaCl concentrations, respectively, were identified by metachromasy. This set of results suggested a polyanionic/sulfated nature for both populations and higher charge density or MW for TgSF as compared to TgFucCS, due to its higher retention in the DEAE Sephacel column. While none of the polysaccharides were positive for sialic acids, the TgFucCS peak was positive for uronic acid. The relatively broad elution profile for the TgSF molecule further indicates a heterogeneous population of sulfated polysaccharide chains.

The polydispersity of the two polysaccharide preparations was examined by native 22% polyacrylamide gel electrophoresis (PAGE) (Figure 1B). The electrophoretic migration of TgFucCS and TgSF was assessed through PAGE comparatively to known standards: low molecular weight heparin (LMWH), UFH, chondroitin sulfate C (CS-C), and the two previously characterized sulfated glycans from the sea cucumber *Holothuria. floridana*, HfFucCS and HfSF.[19] TgFucCS exhibited electrophoretic mobility like UFH (∼15 kDa), while TgSF did not move into the gel, indicating a very high MW for most of its composing chains. The average MWs of the two *T. gemmata*-derived glycans was analyzed by HPSEC-MALS (Figure 1C and 1D). Based on their Rayleigh ratios, molecular masses of TgFucCS (Figure 1C) and TgSF (Figure 1D) were estimated as 17.5 (±3.5%) and 383.3 (±2.1%) kDa, respectively. These average MW values are in consensus with the observed electrophoretic migrations of TgFucCS and TgSF (Figure 1B).

We have confirmed from our results that the elution profile of TgSF after TgFucCS from the DEAE Sephacel column (Figure 1A) was primarily caused by the significant difference

https://doi.org/10.1021/acs.jnatprod.3c00151
J. Nat. Prod. 2023, 86, 1463−1475

Table 1. ^{1}H and ^{13}C Chemical Shifts (ppm) of *T. gemmata*-Derived Fucosylated Chondroitin Sulfate (TgFucCS)[a]

unit	source	$^{1}H1/^{13}C1$	$^{1}H2/^{13}C2$	$^{1}H3/^{13}C3$	$^{1}H4/^{13}C4$	$^{1}H5/^{13}C5$	$^{1}H6,^{1}H6'/^{13}C6$	GalNAc-CH_3
Fuc2,4S (A)	TgFucCS	5.65/96.4[c]	*4.43/75.3*[d]	4.08/66.8	4.88/79.7	4.77/66.4	1.3/16.2	-
Fuc2,4S	[20]	5.69/96.9	4.50/75.6	4.13/67.2	4.84/81.6	4.90/66.7	1.36/16.4	
Fuc4S (B)	TgFucCS	5.38/98.6	3.75/68.6	3.96/69.02	4.74/81.2	4.73/66.5	1.3/16.2	
Fuc4S	[20]	5.40/98.9	3.83/72.3	4.01/67.9	4.75/81.6	4.84/66.7	1.36/16.4	
GalNAc4,6S (N4,6S)	TgFucCS	4.75/100.0	3.97/51.6	3.73/71.9	4.80/75.9	Nd[b]	**4.20**,4.18/66.8	2.01/22.9
GalNAc4,6S	[21]	4.58/100.9	4.07/52.7	3.95/77.9	4.81/77.2	4.0/73.2	**4.33**,4.20/68.5	
GalNAc4S (N4S)	TgFucCS	4.55/100.4	3.97/51.6	3.73/71.9	4.76/75.7	Nd	3.73/61.2	2.01/22.9
GalNAc4S	[21]	4.58/100.9	4.07/52.7	3.95/77.9	4.81/77.2	4.02/76.2	3.81/62.3	
GlcA (U)	TgFucCS	4.66/103.0	3.64/74.8	3.76/77.04	3.95/76.9	3.79/80.7	Nd	
GlcA	[21]	4.48/105.0	3.64/75.0	3.71/78.1	3.96/76.6	3.71/78.1	/176.0	
GlcA (U')	TgFucCS	4.50/104.0	3.38/72.06	3.60/73.8	3.95/76.9	3.79/80.7	Nd	
GlcA	[21]	4.50/105.3	3.38/73.9	3.59/75.2	3.78/82.9	3.70/77.9	/175.9	

[a]The spectra were recorded at 500 MHz in 99.9% D_2O at 50 °C. Chemical shifts are relative to external trimethylsilylpropionic acid 0 ppm for ^{1}H and to methanol for ^{13}C. [b]Not determined. [c]Values in bold indicate glycosylation sites. [d]Values in italics indicate sulfation sites.

in MW of these two sulfated polysaccharides (TgFucCS with ∼17.5 kDa and TgSF with ∼383.3 kDa) and not so much from the sulfation content since both polysaccharides contain similar amounts of disulfated and monosulfated monosaccharides within their chains as further described.

Structural Characterization of TgFucCS. The one-dimensional (1D) ^{1}H NMR spectrum of TgFucCS collected at 50 °C (Figure 2A) revealed a signal profile typical of those reported for fucosylated chondroitin sulfates.[10,13] Diagnostic ^{1}H resonances with chemical shifts (δ_H) in the α-anomeric region (δ_H between 5.65 and 5.25 ppm) indicate the presence of α-Fucose (Fuc) units. ^{1}H resonances of the β-anomeric region (δ_H between 4.75 and 4.40 ppm) indicate the presence of β-*N*-acetylgalactosamine (GalNAc) and β-glucuronic acid (GlcA) units. The upfield methyl region is diagnostic of GalNAc-C$\underline{H}_3$ (δ_H at ∼2.0 ppm) and Fuc-C$\underline{H}_3$ (δ_H at ∼1.3 ppm). Ring-containing ^{1}Hs of the composing monosaccharides resonate with their δ_H varying from 4.9 to 3.3 ppm.

A series of two-dimensional (2D) homonuclear and heteronuclear NMR spectra was acquired for TgFuCS at 50 °C (Figures 2B, 2C, S1, and S2) to achieve complete NMR assignment and consequential assessment of specific structural features such as sulfation patterns, branching, and glycosidic linkages. The α- and β-anomeric ^{1}Hs of the composing residues as identified in the 1D ^{1}H NMR (Figure 2A) and in the $^{1}H-^{13}C$ heteronuclear single quantum coherence (HSQC) (Figure 2C) spectra served as starting points for signal assignments. Assignments of the vicinal carbon-bound ^{1}Hs were achieved using short-range $^{1}H-^{1}H$ connections through correlation spectroscopy (COSY) (Figures S1 and S2). A full spin system of the three residue types (Fuc, GalNAc, and GlcA) was assigned using long-range $^{1}H-^{1}H$ connections through total correlation spectroscopy (TOCSY) (blue spectrum in Figure 2B, green spectra in Figures S1 and S2). Inter-residue glycosidic linkages were established through $^{1}H-^{1}H$ spatial connections in the nuclear Overhauser effect spectroscopy (NOESY) (red spectrum in Figure 2B and orange spectrum in Figure S1). After completing ^{1}H assignments via a combination of COSY and TOCSY spectra, specific ^{13}C chemical shifts (δ_C) were obtained via $^{1}H-^{13}C$ cross-peaks in the $^{1}H-^{13}C$ HSQC spectrum (Figure 2C). Values obtained for the ^{1}H and ^{13}C assignments of TgFucCS are tabulated in Table 1 along with reference values[20,21] of composing monosaccharides from previously published fucosylated chondroitin sulfates.

Two α-Fuc units were identified and denoted as A (δ_{H1} 5.65 ppm) and B (δ_{H1} 5.38 ppm) in Figure 2 and Table 1. Downfield shifts on H2 (δ_H 4.43 ppm) and H4 (δ_H 4.88 ppm) of unit A, as compared to nonsulfated sites (∼0.7 ppm upfield shift), indicated sulfations on both C2 and C4 positions of the Fuc ring A labeled as Fuc2,4S. The spin system of the unit ascribed as B showed a downfield displacement of only H4 (δ_H 4.74 ppm), indicating therefore 4-sulfation at this unit labeled as Fuc4S. The accompanying downfield shifts on respective δ_C values of C2 and/or C4 (of A and B), as compared to nonsulfated sites (7−11 ppm upfield resonances), were also observed in the $^{1}H-^{13}C$ HSQC spectrum of TgFucCS (Figure 2C and Table 1). The integral ratio of two fucosyl units (A:B) obtained from the NMR anomeric signals suggests the occurrence of 65:35% Fuc4S:Fuc2,4S units in TgFucCS.

The strong $^{1}H-^{1}H$ NOE connections observed between H1 of Fuc units and H3 of GlcA (U) (red spectrum in Figure 2B, and Table 1) indicated the presence of fucosyl branches on the GlcA residues attached at the C3 position of the GlcA units. Interestingly, the $^{1}H-^{13}C$ HSQC spectrum of TgFucCS indicated the presence of two GlcA units, one denoted as U (with δ_{H1}/δ_{C1} at 4.66/103.0 ppm) and U′ (with δ_{H1}/δ_{C1} at 4.50/104.0 ppm) existing in an integral ratio of 1:2 U:U′. $^{1}H-^{1}H$ connections observed between H1 of Fuc units (A and B) with H3 of GlcA (U) (δ_H at 3.76 ppm) (red spectrum in Figure 2B, and Table 1) indicated the presence of fucosyl branches on the GlcA residues labeled as U. However, the absence of $^{1}H-^{1}H$ cross-peaks between H1 of either Fuc units and H3 of GlcA (U′) (δ_H at 3.60 ppm) of U′ indicates the occurrence of unbranched (unfucosylated) GlcA residues in TgFucCS. Two types of GalNAc units, labeled as N4,6S and N4S, were also assigned and identified in the 2D spectra (Figures 2C and S2 and Table 1). The respective downfield shifts of H4 and H6 combined, and H4 alone, as compared to nonsulfated sites, indicated the sulfation sites of these two GalNAc units. The resonance integral ratio of 1:2.5 for N4,6S:N4S units reveals the occurrence of 30% and 70% 4,6-disulfated and 6-sulfated GalNAc units in the TgFucCS backbone. Figure 3A displays the structural representation of TgFucCS obtained after the full NMR assignment.

Fucosylated chondroitin sulfates are unique marine heteropolysaccharide GAGs with repeating chondroitin sulfate disaccharide units in their backbone of [→3)-β-GalNAc-(1→4)-β-GlcA-(1→].[17] GlcA residues usually bear the sulfated fucosyl branches attached at its C3 position, and this

https://doi.org/10.1021/acs.jnatprod.3c00151
J. Nat. Prod. 2023, 86, 1463−1475

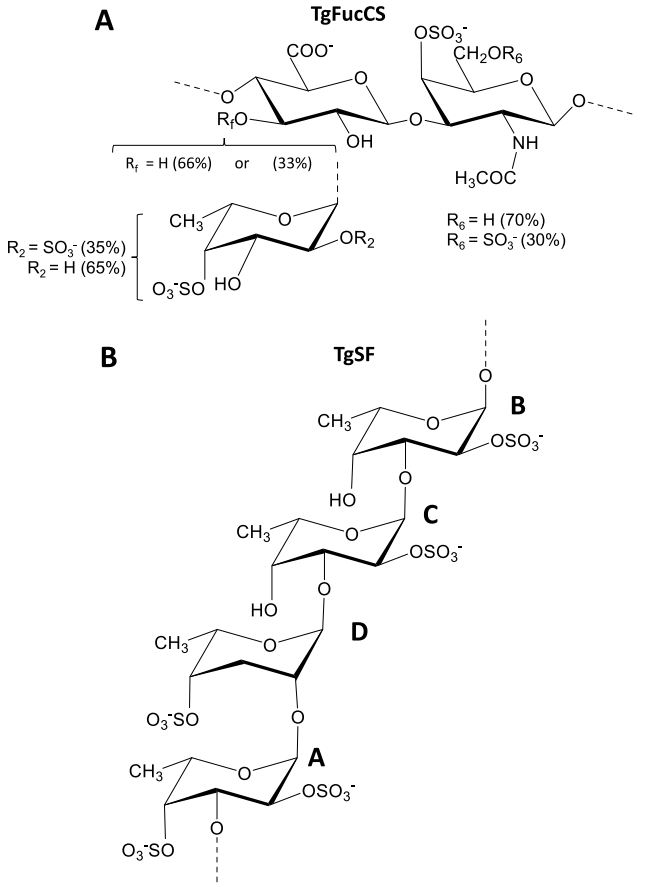

Figure 3. Structural representation of the two sulfated glycans extracted and characterized from the sea cucumber *T. gemmata*: (A) the fucosylated chondroitin sulfate (TgFucCS) and (B) sulfated α-fucan (TgSF) with units assigned as A−D−C−B.

decoration is crucial for many biological actions.[17,22] TgFucCS represents a simple fucosylated chondroitin sulfate type I structure comprising a predominant chondroitin 4-sulfate backbone having monofucosyl branches, Fuc2,4S or Fuc4S, attached to the GlcA unit. As a unique feature, TgFucCS appeared heterogeneous in terms of GlcA composition. Two-thirds of the GlcA content is unbranched (unfucosylated). This feature was also found in the fucosylated chondroitin sulfate of *Cucumaria djakanovi*, in which 60% of its GlcA residues are fucosylated at the C3 position, while the other 40% are unfucosylated.[21] In all, the structures of fucosylated chondroitin sulfates vary in a species-specific way where structural variation relies primarily on sulfation patterns of both the lateral Fuc units and the GalNAc units of the backbones (Figure 3A).

Structural Characterization of TgSF. The 1D ^{1}H NMR spectrum of TgSF displays the typical resonance profile (Figure 4A) reported for sulfated fucans from echinoderms.[13] The ^{1}H signals in the α-anomeric region of TgSF (δ_H between 5.45 and 5.05 ppm) indicated the presence of four major types of α-Fuc units. The cluster of ^{1}H signals with δ_H between 1.2 and 0.8 ppm represented the Fuc-C$\underline{H}_3$. Fuc ring-containing ^{1}H resonances fall in the region of δ_H between 4.9 and 3.5 ppm.

Complete ^{1}H and ^{13}C assignments of TgSF were achieved using the same 2D NMR-based strategy used for TgFucCS. Table 2 displays all δ_H and δ_C values obtained. The four major fucosyl units of TgSF were assigned with letters A−D in the acquired spectra (Figures 4A, 4B, and S3). Unit A exhibits downfield shifts on its H2 (δ_H 4.57 ppm) and H4 (δ_H 4.90 ppm) resonances, while units B and C show a downfield shift only on their H2 (δ_H 4.52 ppm). Unit D showed a downfield shift at their H4 resonances (δ_H 4.54 ppm). These ^{1}H downfield resonances are indicative of sulfation positions, as compared to the typical ∼0.7 ppm ^{1}H upfield shifts of their equivalent nonsulfated ring positions. Corresponding δ_C shifts (Table 2) were also observed at these respective sites. In conclusion, units A−D are Fuc2,4S, Fuc2S, Fuc2S, and Fuc4S, respectively.

Relative NMR integral values indicate the occurrence of 18% for the Fuc2,4S (A) unit, 29% for each Fuc2S (B and C) unit, and 24% for the last Fuc4S unit (D). The glycosidic linkages were established through inter-residue NOE connections obtained in ^{1}H−^{1}H NOESY and ^{1}H−^{13}C HSQC-NOESY (yellow spectrum in Figure 4B and Figure 4C). The following through-space signal pairs were observed: H1 of unit A with H2 of unit D, H1 of unit D with H3 of unit C, H1 of unit C with H3 of unit B, and H1 of unit B with H3 of unit A.

These sites of glycosidic bonds exhibit a significant shift on the ^{13}C scale as seen in the ^{1}H−^{13}C HSQC spectrum (Figure S3C) and from the δ_C values displayed in Table 2. A linear sequence of the tetrasaccharide building block [A−D−C−B] or [Fuc2,4S-Fuc4S-Fuc2S-Fuc2S] could be clearly established, with the presence of a (1→2) linkage between A and D and (1→3) linkages among the other composing disaccharides. The assigned TgSF structure [→3)-α-Fuc2,4S-(1→2)-α-Fuc4S-(1→3)-α-Fuc2S-(1→3)-α-Fuc2S-(1→]$_n$ is displayed in Figure 3B.

Most of the marine invertebrate-derived sulfated fucans are linear in structure and have repeating oligosaccharides units connected by either α(1→3) or α(1→4) glycosidic linkages.[18,23−32] Nonetheless, structures containing branches,[26,33,34] the presence of α(1→2) glycosidic bonds,[33] and additional heterogeneity from glycosidic linkages, such as alternating α(1→3) and α(1→4) linkages within the same chain,[35] have also been reported. The presence of one α(1→2) and three α(1→3) linkages in the TgSF structure is another example of heterogeneity in terms of glycosidic bonds in invertebrate-derived sulfated fucans.

Like fucosylated chondroitin sulfates from sea cucumbers, the structures of sea cucumber sulfated fucans vary also in a species-specific manner, in which sulfation pattern of the Fuc units is the primary structural variation. For the case of the echinoderm tetrasaccharide-repeating 3-linked sulfated α-fucans, sulfation occur at positions O2 and/or O4 of the backbone Fuc units. Examples of these species-specific structures are the sulfated fucans, TgSF derived from *T. gemmata* and HfSF derived from *H. floridana*, whose sulfation patterns (reading frame starting with the 2,4-disulfated units) are [Fuc2,4S-Fuc4S-Fuc2S-Fuc2S] (Figure 3B) and [Fuc2,4S-Fuc-Fuc2S-Fuc2S],[36] respectively. Two other examples of structure are the [Fuc2,4S-Fuc2S-Fuc2S-Fuc4S] from the sea urchin *Lytechinus variegatus*[37] and the [Fuc2,4S-Fuc2S-Fuc2S-Fuc] from the sea cucumber *I. badionotus*.[15] The oligosaccharide building block of these sulfated fucans creates a functional sulfation pattern that plays a key role in their potential biological functions.[14,18]

Anti-SARS-CoV-2 Activity against Wild-Type and Delta Strains. Anti-SARS-CoV-2 activity of the sulfated glycans (UFH, TgFucCS, and TgSF) was examined against baculovirus pseudotyped with wild-type and delta S-proteins in

https://doi.org/10.1021/acs.jnatprod.3c00151
J. Nat. Prod. 2023, 86, 1463−1475

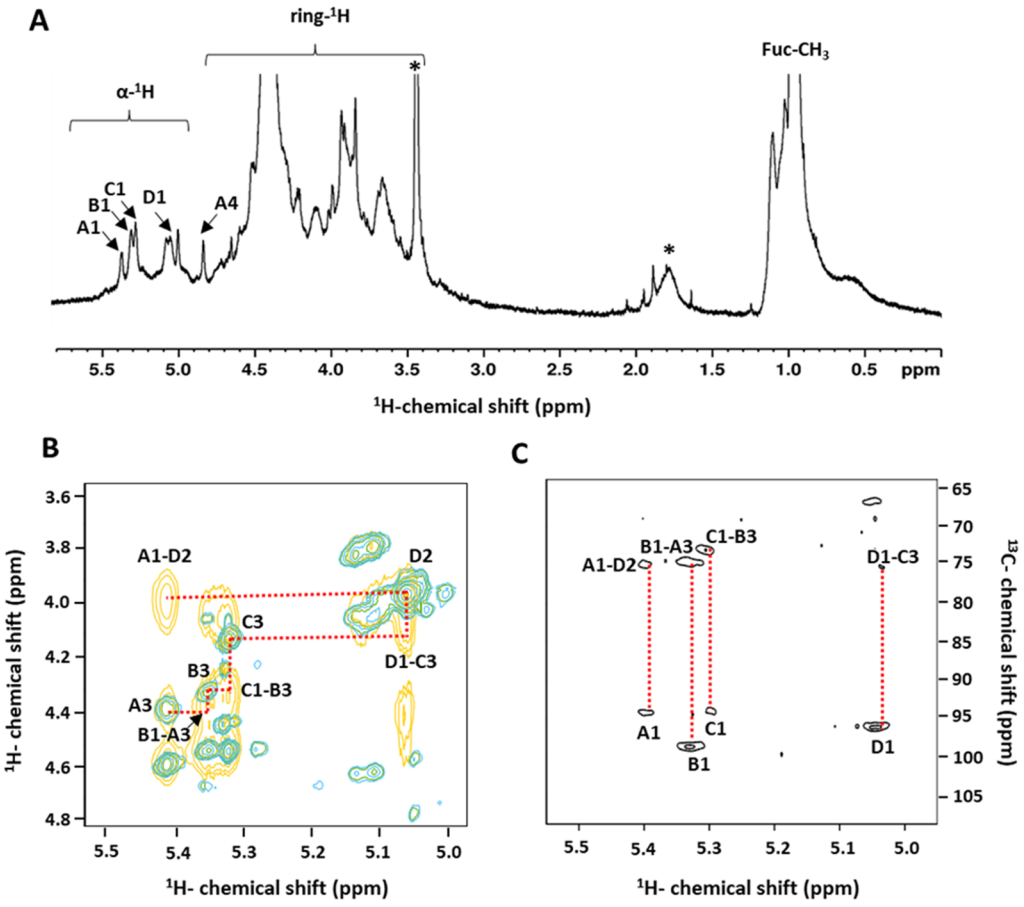

Figure 4. 1D ^{1}H, 2D ^{1}H−^{1}H, and ^{1}H−^{13}C NMR spectra of the composing units of TgSF. (A) ^{1}H NMR spectrum (δ_H expansion 5.8−0.0 ppm) showing diagnostic ^{1}H signals for α-Fuc and Fuc-methyl protons. α-Fuc units are labeled as A (Fuc2,4S), B (Fuc2S), C (Fuc2S), and D (Fuc4S). (B) The overlaid TOCSY (green) and NOESY (yellow) strip (δ_H/δ_H expansions 5.5−5.0/4.8−3.6 ppm) and (D) ^{1}H−^{13}C HSQC-NOESY spectrum (δ_H/δ_C expansions 5.5−3.0/107.5−65.0 ppm) establishing the NOE connections (dashed lines) between four α-Fuc units. Numbers after letters denote the corresponding proton or carbon atoms within the hexose rings. Peak labeled with an asterisk is unknown.

Table 2. ^{1}H and ^{13}C Chemical Shifts (ppm) of *T. gemmata*-Derived Sulfated Fucan (TgSF)[a]

unit	source	^{1}H1/^{13}C1	^{1}H2/^{13}C2	^{1}H3/^{13}C3	^{1}H4/^{13}C4	^{1}H5/^{13}C5	^{1}H6/^{13}C6
Fuc2,4S (A)	TgSF	5.41/93.78[b]	4.57/74.55[c]	4.37/74.32	4.90/80.60	4.31−4.65/67−68.7	0.83−1.19/16.6
Fuc2,4S	[20]	5.40/95.5	4.53/73.7	4.29/73.2	4.89/81.3	4.30/68.2	1.25/16.7
Fuc2S (B)	TgSF	5.35/98.32	4.52/74.98	4.31/78.27	4.05/69.08	4.31−4.65/67−68.7	0.83−1.19/16.6
Fuc2S	[21]	5.38/98.16	4.57/75.92	4.12/77.05	4.12/72.31	4.45/69.51	1.28/18.25
Fuc2S (C)	TgSF	5.32/93.75	4.52/74.90	4.11/72.67	4.22/69.23	4.31−4.65/67−68.7	0.83−1.19/16.6
Fuc2S	[21]	5.38/98.16	4.57/75.92	4.12/77.05	4.12/72.31	4.45/69.51	1.28/18.25
Fuc4S (D)	TgSF	5.05/95.59	3.96/75.70	4.23	4.54/80.2	4.31−4.65/67−68.7	0.83−1.19/16.6
Fuc4S	[23]	5.01/96.0	3.96/68.3	4.17/75.3	4.79/80.2	4.45/68.2	1.2/18.0

[a]The spectra were recorded at 500 MHz in 99.9% D_2O at 50 °C. Chemical shifts are relative to external trimethylsilylpropionic acid 0 ppm for ^{1}H and to methanol for ^{13}C. [b]Values in bold indicate glycosylation sites. [c]Values in italics indicate sulfation sites.

HEK-293T cells using green fluorescent protein (GFP) reporter (Figures 5, S4, and S5).

Table S1 presents the resultant IC_{50} and I_{max} values obtained from the *in vitro* assay. TgSF, exhibited significant anti-SARS-CoV-2 potency comparable to UFH against the wild type (Figure 5A and Table S1). The IC_{50} values (μg/mL) of these glycans were as follows: UFH (0.6 ± 0.03), TgFucCS (6.1 ± 0.6), and TgSF (0.2 ± 0.05). A similar pattern of activity was also observed against the delta variant (Figure 5B and Table S1) based on the respective IC_{50} values of these glycans: UFH (0.2 ± 0.03) and TgSF (0.1 ± 0.03). Like against the wild-type strain, the TgFucCS (IC_{50} = 5.3 ± 0.2) (Table S1) showed the weakest potency among all glycans. The efficacies of all compounds were nearly equal against delta SARS-CoV-2 (Table S1). Interestingly, as opposed to TgFucCS, which exhibited ∼10- and 25-fold lower potency than UFH against the SARS-CoV-2 wild-type and delta strains, TgSF was very similar to UFH and showed the best profile among the two holothurian glycans tested. Sulfated glycans exhibited no toxic effects against HEK-293T cells when tested at the highest concentration of 50 mg/L (Figure 5C).

Sulfated glycans are known to bind to different proteins apart from coagulation factors, which imparts diverse biological properties to this class of carbohydrates.[38] One example of

https://doi.org/10.1021/acs.jnatprod.3c00151
J. Nat. Prod. 2023, 86, 1463−1475

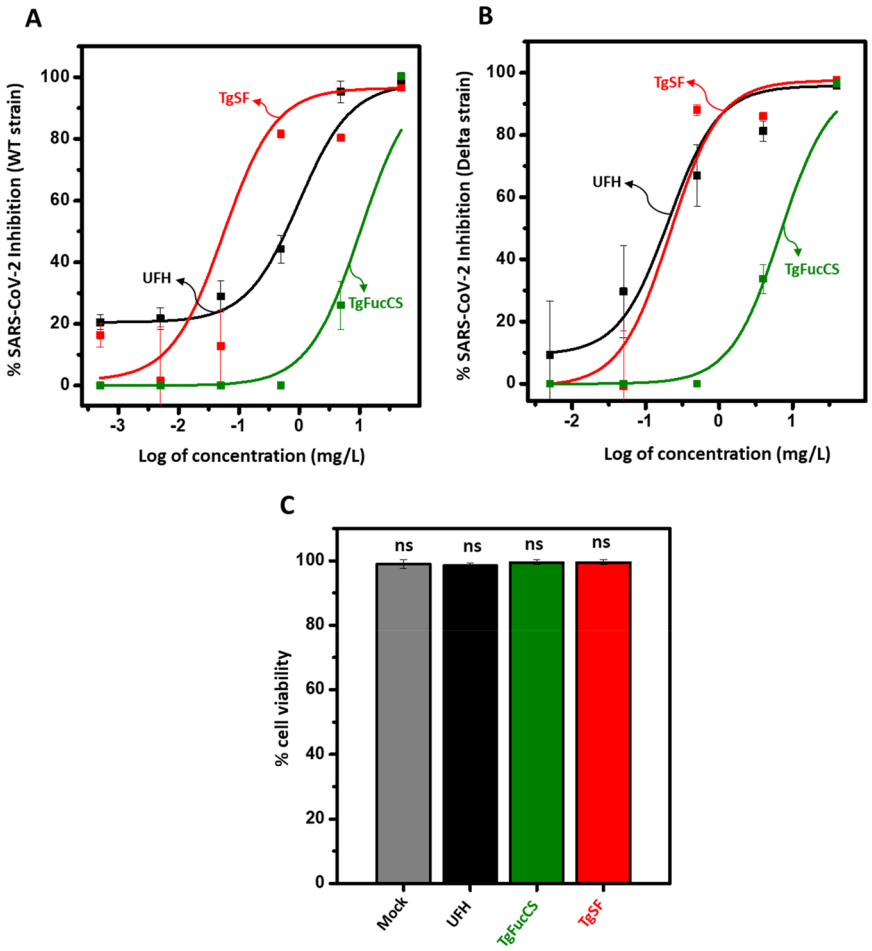

Figure 5. Anti-SARS-CoV-2 activity and cytotoxicity of *T. gemmata*-derived sulfated glycans as compared to UFH. The plotted curve shows percentage inhibition of SARS-CoV-2 (A) wild-type and (B) delta variants in a (log) concentration-dependent manner. (C) Bar plots represent percentage cell viability of HEK-293T-hACE2 cells when treated with sulfated glycans at the highest concentration of 50 mg/L. Each experiment was performed in triplicates, and each point represents the mean ± SD of the triplicated set. ns stands for nonsignificant. Figure shows UFH in black, TgFucCS in green, and TgSF in red.

timely biological relevance is the interaction with viral proteins,[39] including the SARS-CoV-2 S-protein RBD.[6] The global pandemic of 2019 has added SARS-CoV-2 to the list of key viruses under intense research investigations nowadays, particularly regarding the discovery and development of novel anti-SARS-CoV-2 agents. The marine sulfated glycans of unique structural and functional properties have recently awakened interest among researchers. Their anti-SARS-CoV-2 activity arises from their ability to competitively inhibit S-protein RBD binding onto cell surface HS, which is a biochemical mechanism preserved across the emerging SARS-CoV-2 variants. In this work, we demonstrated through cell-based assays using pseudovirus vectors that the TgFucCS and TgSF can exhibit, although at different levels due to their specific structural features, inhibitory properties against two SARS-CoV-2 strains, wild type (Wuhan-Hu-1) and delta (B.1.167.2), with no cytotoxic effects, toward the HEK-293T cells (Figure 5). TgFucCS was the least potent carbohydrate (Table S1), while TgSF presented, in general, the best profile among the two holothurian glycans tested herein.

Anticoagulant Action of Holothurian Sulfated Glycans. Anticoagulant activity of the sulfated glycans was measured by their capabilities to prolong the clotting time in a standard aPTT assay (Figure 6A) and by examining inhibition of thrombin (IIa) (Figure 6B and 6D) or factor Xa (Figure 6C) by antithrombin (AT) (Figure 6B and 6C) or heparin cofactor II (HCII) (Figure 6D) (Table S1). UFH was used as a positive control in all assays, while CS-C was used as negative control in the aPTT (Figure 6A). All holothurian glycans demonstrated aPTT values lower than heparin (black line) in the following decreasing order: TgFucCS (16.5 IU/mg) (green line in Figure 6A) with 11-fold reduction and TgSF (5.7 IU/mg) (red line in Figure 6A) with 30-fold reduction. TgFucCS shows moderate anticoagulant activity, whereas TgSF exhibits weak activity (Figure 6A). In the inhibitory assays using the purified (co)-factors, both TgFucCS and TgSF were weaker than UFH (Table S1). As expected, anticoagulant activity of the holothurian sulfated glycans was more pronounced in the HCII/IIa system (Figure 6D and Table S1), since sulfated fucans and fucosylated chondroitin sulfate are known to exhibit better activity toward the HCII-mediated system.[10,14,15]

An important motif in marine sulfated glycans for anticoagulant activity is the presence of 2,4-disulfation on Fuc units.[14,40,41] The presence of Fuc2,4S units in the TgSF and TgFucCS structure led us to analyze the contribution of this motif in the current results. As observed from the anticoagulant assays (Figure 6), the relatively low Fuc2,4S

https://doi.org/10.1021/acs.jnatprod.3c00151
J. Nat. Prod. 2023, 86, 1463−1475

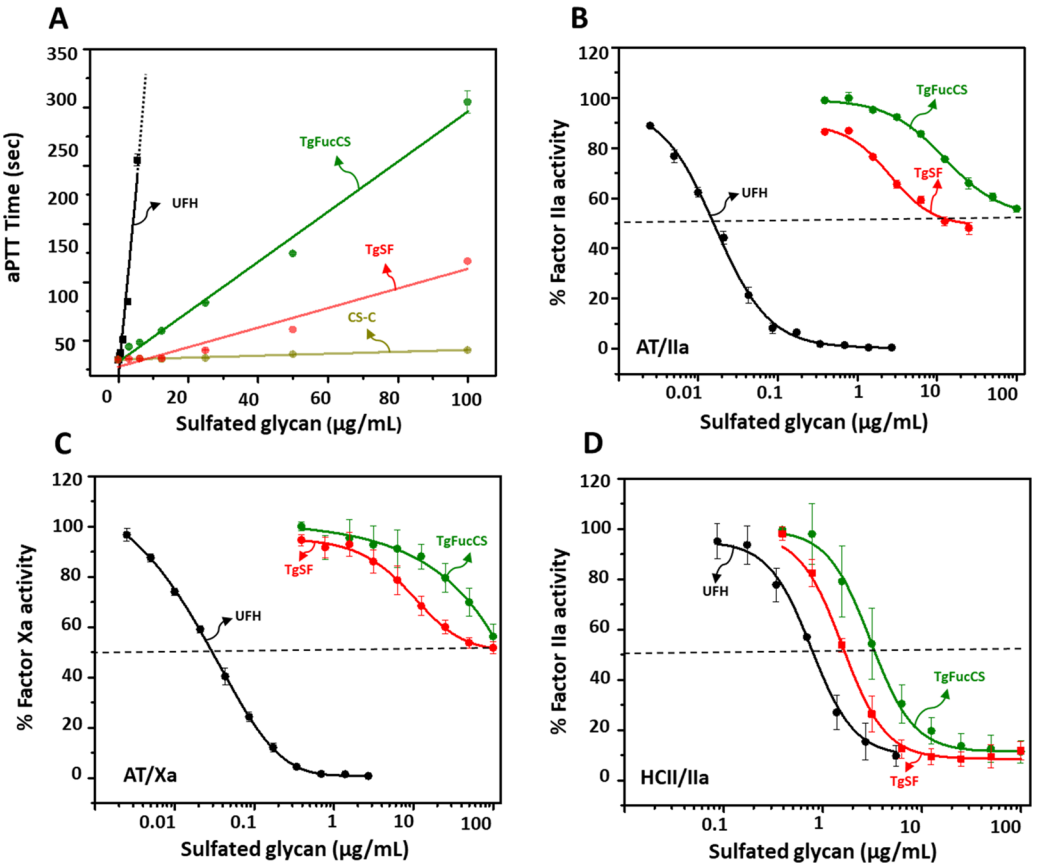

Figure 6. Anticoagulant activity of *T. gemmata*-derived sulfated glycans. (A) aPTT, (B) AT-mediated factor IIa inhibition, (C) AT-mediated factor Xa inhibition, and (D) HCII-mediated factor IIa inhibition. The sulfated glycans examined (in a concentration range up to 100 μg/mL) were UFH (black), CS-C (dark yellow), and the two holothurian sulfated glycans, TgFucCS (green) and TgSF (red). The dotted line in panels B−D indicate the half-maximal inhibitory activity of the glycans. Each experiment was performed in triplicates, and each point in the plotted data represents the mean ± SD of the triplicated set.

content in both TgFucCS and TgSF collaborates with the weaker anticoagulant properties of these two sugars as compared to UFH (Table S1), despite their significant MW and structural differences. The preferable anticoagulant properties of the holothurian sulfated glycans toward the HCII/IIa system are expected and have already been extensively discussed before.[10,14,17,18,22,24,30−33] The combination of low anticoagulant effect with the potent anti-SARS-CoV-2 action of TgSF makes this carbohydrate unique in drug development of the novel anti-SARS-CoV-2 sulfated glycans devoid of the undesirable anticoagulant side-effects. Conversely, the remaining anticoagulant effects of these holothurian sulfated glycans, although weak as primary anticoagulants as compared to UFH, could be also clinically beneficial against associated episodes of accelerated coagulopathies in COVID-19 disease.[42]

Binding Properties of Holothurian Sulfated Glycans to Blood (Co)-Factors and S-Protein RBDs. The ability of holothurian sulfated glycans to competitively inhibit the binding of blood (co)-factors [AT (Figure 7A), HCII (Figure 7B), and IIa (Figure 7C)] and SARS-CoV-2 S-protein RBDs [wild type (Figure 7D), delta (Figure 7E), and omicron (Figure 7F)] to surface heparin was investigated by SPR competition experiments. The decrease in binding of proteins to surface immobilized heparin, in the presence of sulfated glycans, demonstrated the inhibitory potential of the tested glycans. Figure 7A demonstrates almost 100% binding of AT to the surface heparin in the presence of the holothurian sulfated glycans, suggesting very weak interaction of TgFucCS and TgSF to AT. In the case of HCII, both sulfated glycans bind to HCII significantly and cause inhibitory decrease in the HCII binding to surface heparin (Figure 7B and Table S2). The pattern of direct binding to factor IIa (Figure 7C) however was slightly different among these sulfated glycans. TgSF (red bar) showed comparable binding to IIa, like the binding observed for UFH (black bar), while TgFucCS (green bar) showed a reduced binding to IIa (Figure 7C). The inhibitory values are summarized in Table S2, and associated SPR sensorgrams are shown in Figure S6.

Examining the effect of these sulfated glycans on the binding of the three SARS-CoV-2 S-proteins to surface heparin (Figure 7D−F) showed a comparable or improved inhibitory profile of the holothurian glycans in relation to the exogenous UFH. The two marine sulfated glycans presented highly competitive inhibitory properties against wild-type RBD (Figure 7D). Similar effects were also seen against the delta RBD (Figure 7E). Against omicron RBD, however, TgFucCS was significantly weaker than UFH (Figure 7F), while TgSF was more potent than heparin. In all, TgSF showed a great inhibitory profile against all three RBDs (panels D−F of Figure 7, Figure S6, and Table S2). This set of observations matches well with the cell-based anti-SARS-CoV-2 results of Figure 5 against wild-type and delta strains and suggests potential anti-SARS-CoV-2 activity against the omicron variant.

https://doi.org/10.1021/acs.jnatprod.3c00151
J. Nat. Prod. 2023, 86, 1463−1475

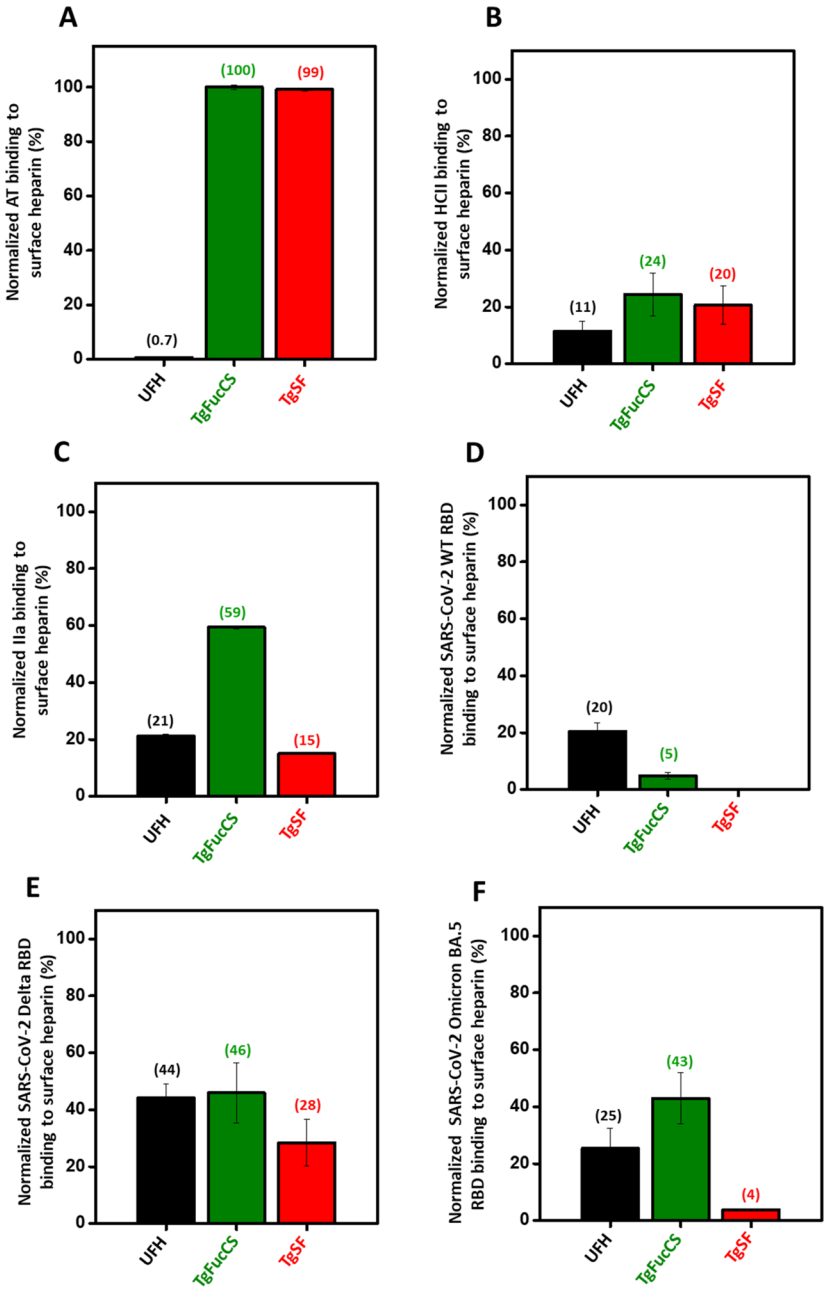

Figure 7. Competitive SPR binding analyses of blood (co)-factors (A−C) and SARS-CoV-2 S-protein RBDs (D−F) to surface heparin in the presence of *T. gemmata*-derived sulfated glycans (TgFucCS, and TgSF) and unfractionated heparin (UFH). The bar plots indicate normalized binding of (A) AT, (B) HCII, (C) thrombin (IIa), (D) wild-type RBD, (E) delta (L542R mutant) RBD, and (F) omicron RBD to a surface heparin-immobilized sensor chip in the presence of UFH (black) and holothurian sulfated glycans, TgFucCS (green) and TgSF (red). The numbers on top of each bar indicate the average normalized binding value obtained in the experiments (different than zero). Each experiment was performed in triplicates, and each point in the plotted data represents the mean ± SD of the triplicated set.

The SPR-based results regarding the binding properties of the holothurian glycans to respective target proteins (AT, HCII, IIa) involved in the coagulation processes and in the SARS-CoV-2 infectivity (wild-type, delta, and omicron S-protein RBDs) (Figure 7) showed great agreement with the *in vitro* activities of these glycans (Figures 5 and 6). For example, the significant reduction in AT binding (Figure 7A) of these sugars as compared to HCII (Figure 7B) and IIa (Figure 7C) mechanistically explains the loss of anticoagulant activity in the AT-mediated systems (Figure 6B and 6C) as opposed to the more pronounced HCII-mediated system (Figure 6D). As the HCII/IIa system has low contribution to the overall anticoagulant pathway, the more pronounced effect of the holothurian glycans toward this system does not significantly reflect in the aPTT prolongation (Figure 6A).

Binding of the holothurian sulfated glycans to the S-protein RBD variants was relatively better than UFH (panels D−F of Figure 7). The lowest binding inhibition of TgFucCS with the wild-type and delta S-protein RBDs (green bars in panels D and E of Figure 7 and Table S2) matches perfectly with the high IC_{50} values seen in the anti-SARS-CoV-2 activities of the two strains (green curves panels A and B of Figure 5 and Table S1). The potent activity of TgSF against the two SARS-CoV-2 strains in the *in vitro* assay (red curves in panels A and B of

https://doi.org/10.1021/acs.jnatprod.3c00151
J. Nat. Prod. 2023, 86, 1463−1475

Figure 5 and Table S1) is mechanistically explained from the great affinity of the TgSF compound in molecular interactions with both wild-type and delta RBDs (red bars in panels D and E in Figure 7 and Table S2). Interestingly, TgSF also showed great affinity for omicron RBD (red bar in panel F in Figure 7 and Table S2), indicating potential inhibitory property against the omicron SARS-CoV-2 variant.

CONCLUSIONS

Our study has isolated and structurally characterized two new sulfated polysaccharides from the sea cucumber *T. gemmata*, TgFucCS (17.5 ± 3.5% kDa) and TgSF (383.3 ± 2.1% kDa). Their anticoagulant, anti-SARS-CoV-2, and cytotoxic effects were analyzed comparatively with UFH. Among the two sulfated glycans studied, TgSF has shown the best balance of high anti-SARS-CoV-2 (against wild-type and delta variants) and low anticoagulant effects. Preliminary SPR analysis has also indicated a great binding property of TgSF to omicron SARS-CoV-2, suggesting therefore a potential effect against this VOC. Further *in vitro* analysis using the cell-based model with omicron must be carried out to prove unequivocally the potential anti-SARS-CoV-2 effect of TgSF against this specific VOC.

EXPERIMENTAL SECTION

General Experimental Procedures. NMR experiments were carried out on a 500 MHz Bruker Avance III HD using a 5 mm BBFO RT probe equipped with a Z gradient. A series of 1D ^{1}H and 2D ^{1}H−^{1}H homonuclear (COSY, TOCSY, and NOESY) or ^{1}H−^{13}C heteronuclear (HSQC and HSQC-NOESY) NMR spectra were recorded. All the experiments were carried out at 50 °C in 5 mm NMR tubes (VWR International) using the solvent deuterium oxide (D_2O) (D 99.90%, Cambridge Isotope Laboratories, Inc.). The acquired NMR data were further processed and analyzed using MestreNova 14.1.0 and TopSpin 4.0 software. For HPSEC-MALS, an Ultimate 3000 high-performance liquid chromatography system (Thermo Scientific, Sunnyvale, CA, USA) connected to the SEC column (Acquity BEH SEC column, 200 Å, 1.7 μm, 4.6 mm × 300 mm, Waters, MA, USA) was used. The eluent was monitored by MALS using a DAWN HELEOS II MALS detector (Wyatt Technologies Co., Santa Barbara, CA, USA). Ammonium acetate and high-performance liquid chromatography grade water were purchased from Fisher Scientific (Fair Lawn, NJ, USA). SPR measurements were performed on a BIAcore 3000, operated using 3000 control and Biaevaluation software, version 4.0.1. (Uppsala, Sweden). Sensor streptavidin (SA) chips were procured from Cytiva (Uppsala, Sweden).

Biological Material. Specimens of the sea cucumbers *T. gemmata* (E-1740) were purchased from Gulf Specimen Marine Laboratories Inc. (Gulf of Mexico, Florida Keys). *T. gemmata* were collected on the low tidal flats in Alligator Harbor, Franklin County, FL. Geographical coordinates of the location are 29.9037651−84.4171537.

Extraction of Sulfated Glycans from *T. gemmata*. The sulfated glycans TgFucCS and TgSF were isolated from the body wall of the sea cucumber *T. gemmata* following a slightly modified protocol to that previously reported.[10] The dry body wall (1 g) of the sea cucumber was digested using papain (0.5 mg/100 mg of dry tissue), 5 mM cysteine, and 5 mM EDTA in 0.1 M sodium acetate buffer, pH 6.0 (2 mL/100 mg of dried tissue), at 60 °C for 24 h. The digested mixture was centrifuged at 4000 rpm for 30 min. The supernatant obtained was precipitated using 2 volumes of 95% ethanol at −20 °C. After 24 h, a precipitate was obtained upon centrifugation at 4000 rpm for 30 min. The precipitate was dissolved in water and dialyzed thrice against distilled water prior to lyophilization to obtain the dry crude extract, yielding a crude mass of 50 mg (5% w/w).

Purification of TgSF and TgFucCS. The dry crude extract (50 mg) was subjected to an anion exchange chromatography (DEAE Sephacel resin, Sigma, St. Louis, MO, USA) column (1 × 20 cm). Polysaccharides were eluted and fractionated using a linear gradient of NaCl (in 0.1 M NaOAc, pH 6.0) from 1 to 3 M at a flow rate of 3 mL/h. The obtained fractions of all the polysaccharides were monitored by the 1,9-dimethylmethylene blue assay.[43] Purified fractions of TgFucCS and TgSF were also assayed for the presence of hexoses,[44] uronic acids,[45] and sialic acids[46] by the Dubois reaction, Carbazole reaction, and Ehlrich assay, respectively. The NaCl concentration was estimated by conductivity. The polysaccharide fractions were pooled and dialyzed thrice against water and lyophilized. The dialyzed sugars were further purified on a size exclusion column (1 × 30 cm) packed with Sephadex G-15 (Sigma, St. Louis, MO, USA). The pure mass yield of TgSF and TgFucCS from the crude extract was approximately 2.5 mg each (5% w/w). The overall pure yield of each sulfated glycan from the dry body tissue was 0.25% w/w.

PAGE. The electrophoretic mobility (polydispersity) of the purified TgFucCS and TgSF was determined by running native PAGE along with the standards LMWH (∼8 kDa), UFH (∼15 kDa), and CS-C (∼60 kDa), and native sulfated glycans were derived from sea cucumber *H. floridana*, HfFucCS and HfSF. A sample amount of 10 μg (in 50% glycerol, 0.5 M Tris, pH 6.8) was loaded on a 1 mm thick discontinuous PAGE system having 4% stacking gel and a 22% resolving gel phase. Electrophoretic migration was performed at 100 V in a 0.25 M Tris-glycine running buffer system. The migration of bands was tracked by 0.02% bromocresol green dye added to one of the lanes of the gel. The gel was stained using 0.1% (w/v) toluidine blue (in 1% acetic acid) for 1 h. Destaining of the gel was done using 1% acetic acid. UFH, LMWH, and CS-C were acquired from Sigma (St. Louis, MO, USA).

HPSEC-MALS of TgFucCS and TgSF. To measure the MWs of TgFucCS and TgSF, HPSEC-MALS was utilized. The samples were injected onto the column and eluted by the isocratic gradient using 50 mM ammonium acetate at the flow rate of 0.2 mL/min. The eluent was monitored by MALS. The instrument was calibrated using polystyrene in toluene for the MALS detector and by bovine serum albumin for MALS-refractive index detectors. Different MW dextrans (∼100 and >500 kDa, Sigma-Aldrich Co.) were used to validate the accuracy of the MW measurement by HPSEC-MALS. The mass measured for >500 kDa dextran was 645.6 kDa (±3.4%), and that of ∼100 kDa dextran was measured to be 103.6 kDa (±2.5).

NMR of TgFucCS and TgSF. The NMR sample of TgFucCS was prepared by dissolving 8 mg of pure polysaccharide in 550 μL of D_2O (99.90%). ^{1}H−^{1}H COSY and ^{1}H−^{1}H TOCSY spectra were acquired using T_1 and T_2 acquisition times of 0.06 and 0.243 s, respectively, and a total number of 128 scans were used for the complete acquisition. The spin-lock time of 80 ms was used in TOCSY. The obtained free induction decay for TOCSY was processed by zero filling and linear prediction prior to Fourier transform. The NOESY spectrum at 150 ms mixing time was used for the assignments of the NOE cross-peaks of TgFucCS. The ^{1}H−^{13}C HSQC spectrum was acquired using T_1 and T_2 acquisition times of 0.121 and 0.005 s, respectively, using 1024 × 256 points. HSQC acquisition was performed via double INEPT transfer using Echo/Antiecho TPPI gradient selection with decoupling during acquisition and using trim pulses in INEPT transfer. The data were processed by zero filling and linear prediction prior to Fourier transform. In all 2D NMR experiments, delays of 5 times the T_1 relaxation times were included between multiple pulses to ensure full recovery of magnetization during the experimentation. The NMR sample of TgSF was prepared by dissolving 7 mg of pure polysaccharide in 550 μL of D_2O (99.90%), and acquisition was performed like TgFuCS with few modifications. ^{1}H−^{1}H COSY and ^{1}H−^{1}H TOCSY spectra were acquired using a total number of 128 scans and 256 scans, respectively. A spin-lock time of 100 ms was set for TOCSY. The NOESY spectrum with 512 scans was acquired with 250 ms mixing time. The ^{1}H−^{13}C HSQC spectrum of TgSF were acquired using T_1 and T_2 acquisition times of 0.121 and 0.005 s, respectively, using 1024

https://doi.org/10.1021/acs.jnatprod.3c00151
J. Nat. Prod. 2023, 86, 1463−1475

× 128 points. The $^{1}H-^{13}C$ HSQC-NOESY spectrum was acquired using 2048 × 256 points, with a 150 ms mixing time and 256 scans. The data were processed by zero filling and linear prediction prior to Fourier transform.

aPTT. aPTT was performed by incubating 90 μL of plasma with 10 μL of varying concentrations of holothurian sulfated glycans (TgFucCS and TgSF) or UFH at 37 °C for 3 min. aPTT reagent (100 μL) was then added to the above mixture and incubated for 5 min at 37 °C. Clotting time was measured immediately following the addition of 0.025 M $CaCl_2$ (100 μL). The aPTT readout was measured in seconds. UFH (180 IU/mg) was used as a positive control. The measurements were performed on an Amelung Coagulometer KC4A.

AT/HCII-Dependent IIa/Xa Inhibition. Holothurian sulfated glycans (TgFucCS and TgSF) were assayed for their serpin-mediated inhibitory activity. An assay was performed against factor IIa and Xa using an effective concentration of 10 nM of AT or HCII, 2 nM of IIa or factor Xa, and 0−100 μg/mL of sulfated glycans in 100 μL of TS/PEG buffer (0.02 M Tris/HCl, 0.15 M NaCl, and 1.0 mg/mL polyethylene glycol 8000, pH 7.4) as reported earlier.[47] Sulfated glycans (10 μL) at serial diluted concentrations were dispensed in the 96-well microtiter plate, followed by the addition of 40 μL of AT (25 nM) or HCII (25 nM). The reaction was initiated by adding 50 μL of IIa (4 nM) or Xa (4 nM). The plate was then immediately incubated at 37 °C for 1 min, which was followed by the addition of 25 μL of chromogenic substrate S-2238 (Chromogenix, AB, Mondal, Sweden) for IIa or CS-11(32) (Aniara Diagnostica, West Chester, OH, USA) for factor Xa. The absorbance (Abs) was then measured at 405 nm for 300 s at an interval of 15 s. Wells without sulfated glycans served as control and were considered 100% for IIa/Xa activity. The residual IIa/Xa activity in glycan-treated wells was calculated relative to that observed in the case of control wells. UFH (180 IU/mg) was used in all the assays as a positive control. All the aPTT assay reagents were procured from Thermo Fisher Scientific (Waltham, MA, USA), and the coagulation factors Xa, IIa, AT, and HCII were from Haematologic Technologies. All the assays were performed three times. Calculated IC_{50} values represent mean ± SD obtained from the triplicated measurements.

Viral Inhibition. The virus inhibitor screening was done on human embryonic kidney cells (HEK-293T) expressing human angiotensin-converting enzyme 2 (HEK-293T-hACE2 cell line, BEI Resources #NR-52511) plated in a 96-well tissue culture plate using a baculovirus pseudotyped with SARS-CoV-2 delta-variant and wild-type S-protein containing a green fluorescent reporter [Montana Molecular, #C1123G].[11,13] Virus titers were confirmed by enumerating GFP-positive transduced cells in a dilution under a fluorescence microscope (EVOS-FL, Thermo Fisher Scientific) and multiplying by the dilution factor and the volume plated. Serial dilutions (50, 5, 0.5, 0.05, 0.005, and 0.0005 mg/L) of the test sulfated glycans (TgFucCS, TgSF, and UFH) were made in DMEM in triplicates to the final volume of 100 μL in each well. The controls used were unfractionated heparin at 50 mg/L and mock-treated cells. The 2.5 μL of the pseudotyped virus stock (2×10^{10} units per mL) was mixed with the test compounds and incubated for 1 h, which was then laid over HEK-293T-hACE2 cells plated in a 96-well plate along with 2 mM of sodium butyrate. The plate was then incubated for 60 h, and the assay was read on a Cytation 5 automated fluorescence microscope after fixing with 3.7% formaldehyde. The relative IC_{50} values were calculated in Prism 9 (Graphpad Inc.) by plotting normalized values from the assay against the concentrations (log) of sulfated glycans and controls and analyzing by nonlinear regression to fit a dose−response curve using the least-squares method considering each replicate value as an individual point. Each experiment was performed in triplicates. Plotted values represent the mean ± SD.

Cytotoxicity. Cytotoxic activity of sulfated glycans (TgFucCS, TgSF, and UFH) was determined against HEK-293T-hACE2 cells seeded in 12-well tissue culture plates following the protocol reported earlier. The confluent HEK-293T-hACE2 cells were treated with sulfated glycans at a final concentration of 50 mg/L along with 2 mM sodium butyrate. The treated cells were harvested after 60 h of incubation and examined via a trypan blue exclusion assay for viability. Assay readout was measured on a TC20 automated cell counter (BioRad) according to the manufacturer's protocol. The assay was performed in triplicates, and the values are plotted as mean ± SD of % live cells.

Preparation of Heparin Sensor Chip for SPR. Heparin (2 mg) and amine-PEG3-Biotin (2 mg, Pierce, Rockford, IL, USA) were dissolved in 200 μL of H_2O, and 10 mg $NaCNBH_3$ was added. The reaction mixture was heated at 70 °C for another 24 h; after that a further 10 mg of $NaCNBH_3$ was added, and the reaction was heated at 70 °C for another 24 h. After cooling to room temperature, the mixture was desalted with the spin column (3000 MWCO). Biotinylated heparin was collected, freeze-dried, and used for SA chip preparation. The biotinylated heparin was immobilized to an SA chip based on the manufacturer's protocol. In brief, a 20 μL solution of biotinylated heparin (0.1 mg/mL) in HBS-EP running buffer was injected over flow cell 2 (FC2) of the SA chip at a flow rate of 10 μL/min. The successful immobilization of heparin was confirmed by the observation of a ∼200 resonance unit (RU) increase in the sensor chip. The control flow cell (FC1) was prepared by 1 min injection with saturated biotin.

Competitive Solution SPR. Solution competition study between surface heparin and different soluble holothurian sulfated glycans (TgFucCS, TgSF, and UFH) was performed using SPR. In brief, protein samples SARS-CoV-2 S-Protein RBDs (wild type), mutants [L542 (delta) and omicron (BA.5 subvariant)], and coagulation (co)-factors (IIa, AT, and HCII) mixed with sulfated glycans (100 μg/mL) in HBS-EP buffer were injected over a heparin chip at a flow rate of 30 μL/min, respectively. After each run, the chip was regenerated with a 2 M NaCl injection. For each set of competition experiments on SPR, a control experiment (with only protein) was performed. Normalized binding of the proteins to surface heparin in the presence of different sulfated glycans was determined with respect to control values. This was calculated by dividing the obtained RU values of each experiment (using various glycans) by the control values. Each experiment was repeated in triplicates, and results were presented as the mean ± SD of the three experiments. SARS-CoV-2 S-protein RBD (wild type) and L542 mutant (delta) were provided by Prof. John Bates, University of Mississippi Medical Center. Omicron RBD (BA.2 subvariant) was purchased from Sino Biological Inc.

■ ASSOCIATED CONTENT

Data Availability Statement

The authors declare that the data supporting the findings of this study are available within the article and its Supporting Information file. Additional data can be provided from the corresponding author upon request.

Supporting Information

The Supporting Information is available free of charge at https://pubs.acs.org/doi/10.1021/acs.jnatprod.3c00151.

Additional 2D NMR spectra of TgFucCS and TgSF; fluorescence micrographs showing SARS-CoV-2 wild-type and delta titers; tables presenting IC_{50} and I_{max} values of biological activities; SPR sensorgrams (PDF)

■ AUTHOR INFORMATION

Corresponding Author

Vitor H. Pomin − *Department of BioMolecular Sciences and Research Institute of Pharmaceutical Sciences, School of Pharmacy, University of Mississippi, Oxford, Mississippi 38677, United States;* orcid.org/0000-0002-5015-8880; Phone: +01-662-915-3114; Email: vpomin@olemiss.edu

https://doi.org/10.1021/acs.jnatprod.3c00151
J. Nat. Prod. 2023, 86, 1463−1475

Authors

Rohini Dwivedi − *Department of BioMolecular Sciences, University of Mississippi, Oxford, Mississippi 38677, United States*

Marwa Farrag − *Department of BioMolecular Sciences, University of Mississippi, Oxford, Mississippi 38677, United States; Department of Pharmacognosy, Faculty of Pharmacy, Assiut University, Assiut 71515, Egypt*

Poonam Sharma − *Center for Immunology and Microbial Research, Department of Cell and Molecular Biology, University of Mississippi Medical Center, Jackson, Mississippi 39216, United States*

Deling Shi − *Center for Biotechnology and Interdisciplinary Studies, Rensselaer Polytechnic Institute, Troy, New York 12180, United States*

Anter A. Shami − *Department of BioMolecular Sciences, University of Mississippi, Oxford, Mississippi 38677, United States*

Sandeep K. Misra − *Department of BioMolecular Sciences, University of Mississippi, Oxford, Mississippi 38677, United States;* orcid.org/0000-0001-9165-3987

Priya Ray − *Center for Immunology and Microbial Research, Department of Cell and Molecular Biology, University of Mississippi Medical Center, Jackson, Mississippi 39216, United States*

Jayanti Shukla − *Center for Immunology and Microbial Research, Department of Cell and Molecular Biology, University of Mississippi Medical Center, Jackson, Mississippi 39216, United States*

Fuming Zhang − *Center for Biotechnology and Interdisciplinary Studies, Rensselaer Polytechnic Institute, Troy, New York 12180, United States;* orcid.org/0000-0003-2803-3704

Robert J. Linhardt − *Center for Biotechnology and Interdisciplinary Studies, Rensselaer Polytechnic Institute, Troy, New York 12180, United States;* orcid.org/0000-0003-2219-5833

Joshua S. Sharp − *Department of BioMolecular Sciences, Department of Chemistry and Biochemistry, and Research Institute of Pharmaceutical Sciences, School of Pharmacy, University of Mississippi, Oxford, Mississippi 38677, United States;* orcid.org/0000-0002-0115-0276

Ritesh Tandon − *Department of BioMolecular Sciences, University of Mississippi, Oxford, Mississippi 38677, United States; Center for Immunology and Microbial Research, Department of Cell and Molecular Biology, University of Mississippi Medical Center, Jackson, Mississippi 39216, United States; Department of Medicine, University of Mississippi Medical Center, Jackson, Mississippi 39216, United States*

Complete contact information is available at: https://pubs.acs.org/10.1021/acs.jnatprod.3c00151

Author Contributions

V. H. P. conceptualization; R. D., P. S., D. S., A. A. S., S. K. M., F. Z., and V. H. P. formal analysis; R. D., P. S., D. S., A. A. S., S. K. M., P. R., J. S., and F. Z. investigation; M. F., F. Z., R. J. L., J. S. S., R. T., and V. H. P. resources; R. D., P. S., D. S., A. A. M., S. K. M., and F. Z. data curation; R. D. and V. H. P. writing−original draft; R. D., P. S., D. S., S. K. M., F. Z., and V. H. P. validation; R. D., R. and V. H. P. writing−review and editing; V. H. P. visualization; F. Z., R. J. L., J. S. S., R. T., and V. H. P. supervision; V. H. P. project administration; F. Z., R. J. L., J. S. S., R. T., and V. H. P. funding acquisition.

Funding

This work was supported by funds from the National Institutes of Health [1P20GM130460-01A1-7936 (J. S. S. and V. H. P), 1R03NS110996-01A1 (J. S. S. and V. H. P.), and (1R01DE031928-01A1) (R. T.)], NASA (80NSSC19K1603) (R. T.), and the University of Mississippi. This work was also supported by NIH (AG069039-01 and DK111958) and GlycoMIP, a National Science Foundation Materials Innovation Platform, funded through the Cooperative Agreement DMR-1933525 to R. J. L. and F. Z. The content of the information does not necessarily reflect the position or the policy of the sponsors, and no official endorsement should be inferred.

Notes

The authors declare no competing financial interest.

■ ACKNOWLEDGMENTS

The authors are deeply grateful to the University of Mississippi for providing the needed facilities for the research. The authors are also thankful to Maggie C. Taylor for helping in the crude extraction of polysaccharides from the *T. gemmata* body wall.

■ REFERENCES

(1) Aleem, A.; Akbar Samad, A. B.; Slenker, A. K. In *StatPearls*; StatPearls Publishing: Treasure Island, FL, 2022.

(2) Rochman, N. D.; Wolf, Y. I.; Faure, G.; Mutz, P.; Zhang, F.; Koonin, E. V. *Proc. Natl. Acad. Sci. U. S. A.* **2021**, *118* (29), No. e2104241118.

(3) Minkoff, J. M.; tenOever, B. *Nat. Rev. Microbiol* **2023**, 1−17.

(4) Peacock, T. P.; Penrice-Randal, R.; Hiscox, J. A.; Barclay, W. S. *J. Gen. Virol.* **2021**, *102* (4), 001584.

(5) Peng, H.; Fu, Y.-X *Cell Res.* **2023**, *33* (1), 5−6.

(6) Clausen, T. M.; Sandoval, D. R.; Spliid, C. B.; Pihl, J.; Perrett, H. R.; Painter, C. D.; Narayanan, A.; Majowicz, S. A.; Kwong, E. M.; McVicar, R. N.; Thacker, B. E.; Glass, C. A.; Yang, Z.; Torres, J. L.; Golden, G. J.; Bartels, P. L.; Porell, R. N.; Garretson, A. F.; Laubach, L.; Feldman, J.; Yin, X.; Pu, Y.; Hauser, B. M.; Caradonna, T. M.; Kellman, B. P.; Martino, C.; Gordts, P. L. S. M.; Chanda, S. K.; Schmidt, A. G.; Godula, K.; Leibel, S. L.; Jose, J.; Corbett, K. D.; Ward, A. B.; Carlin, A. F.; Esko, J. *Cell* **2020**, *183* (4), 1043−1057.e15.

(7) Wang, L.; Wu, Y.; Yao, S.; Ge, H.; Zhu, Y.; Chen, K.; Chen, W.; Zhang, Y.; Zhu, W.; Wang, H.; Guo, Y.; Ma, P.; Ren, P.; Zhang, X.; Li, H.; Ali, M. A.; Xu, W.; Jiang, H.; Zhang, L.; Zhu, L.; Ye, Y.; Shang, W.; Bai, F. *Acta Pharmacol. Sin.* **2022**, *43* (4), 788−796.

(8) Choudhary, V.; Gupta, A.; Sharma, R.; Parmar, H. S. *J. Proteins Proteomics* **2021**, *12* (4), 257−270.

(9) Kim, S. B.; Zoepfl, M.; Samanta, P.; Zhang, F.; Xia, K.; Thara, R.; Linhardt, R. J.; Doerksen, R. J.; McVoy, M. A.; Pomin, V. H. *J. Biol. Chem.* **2022**, *298* (5), 101856.

(10) Dwivedi, R.; Samanta, P.; Sharma, P.; Zhang, F.; Mishra, S. K.; Kucheryavy, P.; Kim, S. B.; Aderibigbe, A. O.; Linhardt, R. J.; Tandon, R.; Doerksen, R. J.; Pomin, V. H. *J. Biol. Chem.* **2021**, *297* (4), 101207.

(11) Tandon, R.; Sharp, J. S.; Zhang, F.; Pomin, V. H.; Ashpole, N. M.; Mitra, D.; McCandless, M. G.; Jin, W.; Liu, H.; Sharma, P.; Linhardt, R. *J. Virol.* **2021**, *95* (3), No. e01987-20.

(12) Guimond, S. E.; Mycroft-West, C. J.; Gandhi, N. S.; Tree, J. A.; Le, T. T.; Spalluto, C. M.; Humbert, M. V.; Buttigieg, K. R.; Coombes, N.; Elmore, M. J.; Wand, M.; Nyström, K.; Said, J.; Setoh, Y. X.; Amarilla, A. A.; Modhiran, N.; Sng, J. D. J.; Chhabra, M.; Young, P. R.; Rawle, D. J.; Lima, M. A.; Yates, E. A.; Karlsson, R.; Miller, R. L.; Chen, Y.-H.; Bagdonaite, I.; Yang, Z.; Stewart, J.; Nguyen, D.; Laidlaw, S.; Hammond, E.; Dredge, K.; Wilkinson, T. M.

A.; Watterson, D.; Khromykh, A. A.; Suhrbier, A.; Carroll, M. W.; Trybala, E.; Bergström, T.; Ferro, V.; Skidmore, M. A.; Turnbull, J. E. *ACS Cent. Sci.* **2022**, *8* (5), 527−545.
(13) Dwivedi, R.; Sharma, P.; Farrag, M.; Kim, S. B.; Fassero, L. A.; Tandon, R.; Pomin, V. H. *Glycobiology* **2022**, *32* (10), 849−854.
(14) Pomin, V. H.; Mourão, P. A. S *Front. Cell. Infect. Microbiol.* **2014**, *4*, 33.
(15) Chen, S.; Hu, Y.; Ye, X.; Li, G.; Yu, G.; Xue, C.; Chai, W. *Biochim. Biophys. Acta* **2012**, *1820* (7), 989−1000.
(16) Tamori, M.; Ishida, K.; Matsuura, E.; Ogasawara, K.; Hanasaka, T.; Takehana, Y.; Motokawa, T.; Osawa, T. *PLoS One* **2016**, *11* (5), No. e0155673.
(17) Pomin, V. H. *Mar. Drugs* **2014**, *12* (1), 232−254.
(18) Pomin, V. H. *Biochim. Biophys. Acta* **2012**, *1820* (12), 1971−1979.
(19) Shi, D.; Qi, J.; Zhang, H.; Yang, H.; Yang, Y.; Zhao, X. *Int. J. Biol. Macromol.* **2019**, *132*, 738−747.
(20) Soares, P. A. G.; Ribeiro, K. A.; Valente, A. P.; Capillé, N. V.; Oliveira, S.-N. M. C. G.; Tovar, A. M. F.; Pereira, M. S.; Vilanova, E.; Mourão, P. A. S *Glycobiology* **2018**, *28* (8), 565−579.
(21) Ustyuzhanina, N. E.; Bilan, M. I.; Panina, E. G.; Sanamyan, N. P.; Dmitrenok, A. S.; Tsvetkova, E. A.; Ushakova, N. A.; Shashkov, A. S.; Nifantiev, N. E.; Usov, A. I. *Mar. Drugs* **2018**, *16* (10), 389.
(22) Pomin, V. H. *Curr. Med. Chem.* **2015**, *22* (36), 4166−4176.
(23) Shang, F.; Mou, R.; Zhang, Z.; Gao, N.; Lin, L.; Li, Z.; Wu, M.; Zhao, J. *Carbohydr. Polym.* **2018**, *195*, 257−266.
(24) He, W.; Sun, H.; Su, L.; Zhou, D.; Zhang, X.; Shanggui, D.; Chen, Y. *Int. J. Biol. Macromol.* **2020**, *164*, 87−94.
(25) Ma, Y.; Gao, N.; Zuo, Z.; Li, S.; Zheng, W.; Shi, X.; Liu, Q.; Ma, T.; Yin, R.; Li, X.; Zhao, J. *Int. J. Biol. Macromol.* **2021**, *186*, 535−543.
(26) Zheng, W.; Zhou, L.; Lin, L.; Cai, Y.; Sun, H.; Zhao, L.; Gao, N.; Yin, R.; Zhao, J. *Mar. Drugs* **2019**, *17* (4), 198.
(27) Kariya, Y.; Mulloy, B.; Imai, K.; Tominaga, A.; Kaneko, T.; Asari, A.; Suzuki, K.; Masuda, H.; Kyogashima, M.; Ishii, T. *Carbohydr. Res.* **2004**, *339* (7), 1339−1346.
(28) Yang, W.; Cai, Y.; Yin, R.; Lin, L.; Li, Z.; Wu, M.; Zhao, J. *Int. J. Biol. Macromol.* **2018**, *115*, 1055−1062.
(29) Ustyuzhanina, N. E.; Bilan, M. I.; Dmitrenok, A. S.; Tsvetkova, E. A.; Nikogosova, S. P.; Hang, C. T. T.; Thinh, P. D.; Trung, D. T.; Van, T. T. T.; Shashkov, A. S.; Usov, A. I.; Nifantiev, N. E. *Mar. Drugs* **2022**, *20* (6), 380.
(30) Berteau, O.; Mulloy, B. *Glycobiology* **2003**, *13* (6), 29R−40R.
(31) Pomin, V. H.; Mourão, P. A. S *Glycobiology* **2008**, *18* (12), 1016−1027.
(32) Pomin, V. H. *Mar. Drugs* **2012**, *10* (4), 793−811.
(33) Wu, M.; Xu, L.; Zhao, L.; Xiao, C.; Gao, N.; Luo, L.; Yang, L.; Li, Z.; Chen, L.; Zhao, J. *Mar. Drugs* **2015**, *13* (4), 2063−2084.
(34) Yu, L.; Xue, C.; Chang, Y.; Hu, Y.; Xu, X.; Ge, L.; Liu, G. *Food Chem.* **2015**, *180*, 71−76.
(35) Gao, N.; Chen, R.; Mou, R.; Xiang, J.; Zhou, K.; Li, Z.; Zhao, J. *Int. J. Biol. Macromol.* **2020**, *164*, 3421−3428.
(36) Kim, S. B.; Farrag, M.; Mishra, S. K.; Misra, S. K.; Sharp, J. S.; Doerksen, R. J.; Pomin, V. H. *Carbohydr. Polym.* **2023**, *301*, 120316.
(37) Pomin, V. H.; Pereira, M. S.; Valente, A.-P.; Tollefsen, D. M.; Pavão, M. S. G.; Mourão, P. A. S *Glycobiology* **2005**, *15* (4), 369−381.
(38) Esko, J. D.; Linhardt, R. J. In *Essentials of Glycobiology*, 2nd ed.; Cold Spring Harbor Laboratory Press, 2009, Chapter 35.
(39) Cagno, V.; Tseligka, E. D.; Jones, S. T.; Tapparel, C. *Viruses* **2019**, *11* (7), 596.
(40) Pomin, V. H. *Glycoconj. J.* **2014**, *31* (5), 341−344.
(41) Fonseca, R. J. C.; Santos, G. R. C.; Mourão, P. A. S *Thromb. Haemost.* **2009**, *102* (5), 829−836.
(42) Becker, R. C. *J. Thromb. Thrombolysis* **2020**, *50* (1), 54.
(43) Farndale, R. W.; Sayers, C. A.; Barrett, A. J. *Connect. Tissue Res.* **1982**, *9* (4), 247−248.
(44) DuBois, M.; Gilles, K. A.; Hamilton, J. K.; Rebers, P. A.; Smith, F. *Anal. Chem.* **1956**, *28* (3), 350−356.
(45) Cesaretti, M.; Luppi, E.; Maccari, F.; Volpi, N. *Carbohydr. Polym.* **2003**, *54* (1), 59−61.
(46) Lovekamp, J. J.; Simionescu, D. T.; Mercuri, J. J.; Zubiate, B.; Sacks, M. S.; Vyavahare, N. R. *Biomaterials* **2006**, *27* (8), 1507−1518.
(47) Vasconcelos, A. A.; Sucupira, I. D.; Guedes, A. L.; Queiroz, I. N.; Frattani, F. S.; Fonseca, R. J.; Pomin, V. H. *Mar. Drugs* **2018**, *16* (9), 304.

https://doi.org/10.1021/acs.jnatprod.3c00151
J. Nat. Prod. 2023, 86, 1463−1475